Energy decomposition analysis in free-surface flows: road-map for the direct computation of wave breaking dissipation

A. Colagrossi
CNR-INSEAN
Rome, Italy

B. Bouscasse
CNR-INSEAN (Rome,Italy)
Aeronautics Department (ETSIA),
Technical University of Madrid (UPM),
Madrid, Spain

A. Souto-Iglesias
Naval Architecture Department (ETSIN),
Technical University of Madrid (UPM),
Madrid, Spain

***Abstract*—A viscous free-surface flow energy decomposition analysis is conducted in the present paper. In the presence of a free surface, the viscous dissipation for a Newtonian liquid can be decomposed into two terms: an enstrophy component and a free-surface deformation component. Equations for such terms in the weakly compressible SPH (WCSPH) formalism are devised. They require the discretization of a volume and a surface integral, respectively. Applying energy conservation, a double-checking of the free surface term is developed and applied, confirming the quality of the surface integral SPH evaluation, even in the presence of moderately fragmented free surface. Application to a large amplitude standing wave with breaking is presented.**

I. Introduction

Breaking waves induced mechanical energy dissipation is important for the design of earthquake sloshing dampers for buildings and bridges. Its modelling is an extremely challenging problem with mesh based VOF techniques due to the diffusion at the fragmented interface. Sun & Fujino [1] looked at the topic by semi-empirical methods and Iafratti [2] analyzed the vorticity generation during dam-breaks. Bouscasse et al. [3], [4] demonstrated the importance of wave breaking dissipation in damping angular motions, by performing an analogy with a hydraulic jump. However, insight on the dissipation mechanisms due to breaking is yet an open problem.

Colagrossi et al. [5] conducted a decomposition analysis of mechanical energy dissipation contributors in small amplitude gravity waves. That analysis is pursued here by extending it to large amplitude waves with wave breaking and by directly evaluating the free surface terms through SPH summations.

The paper is organized as follows: physical problem, governing equations and boundary conditions are first presented; the dissipation sources are then individualized through volume and surface integrals; the implementation of these integrals in SPH is presented and applied to a standing wave, discussing the influence of its amplitude, the fluid viscosity and the onset of breaking influence. Finally some conclusions are drawn.

II. Physical problem and governing equations

A. Governing equations

A fluid domain Ω is considered whose boundary, $\partial\Omega$, consists of a free surface, $\partial\Omega_F$, and of a solid boundary $\partial\Omega_B$ (Fig. 1); in practical applications periodic boundaries may be also considered. Since WCSPH will be employed at the discrete level, compressible Navier-Stokes conservation equations are of application:

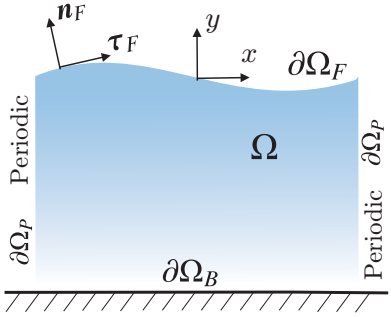

Fig. 1. Layout of the physical domain

$$\begin{cases} \dfrac{D\rho}{Dt} = -\rho\,\mathrm{div}(\boldsymbol{u})\,, \\ \dfrac{D\boldsymbol{u}}{Dt} = \boldsymbol{f} + \dfrac{\mathrm{div}(\mathbb{T})}{\rho}\,, \end{cases} \tag{II.1}$$

where D/Dt represents the Lagrangian derivative, $\boldsymbol{u}$ the flow velocity, ρ the fluid density, $\mathbb{T}$ the stress tensor, $\mathbb{D}$ the rate of strain tensor and $\boldsymbol{f}$ is a generic specific body force. Thermal conductivity effects are here neglected. The pressure p is linked to density and internal energy through a state equation which changes depending on the nature of the fluid (gas or liquid). For example in the weakly-compressible regime for a liquid a simple adiabatic linear state equation can be used to link the pressure and density fields:

$$p = c_0^2\,(\rho - \rho_0) \tag{II.2}$$

where, c_0 is the speed of sound, supposed constant, and ρ_0 and p_0 are respectively the density and the pressure of the fluid at rest. The weakly-compressible regime (density variation smaller than $0.01\rho_0$) is expected if the Mach number of the flow remains enough small during the time evolution (see *e.g.* [6]).

The fluid is assumed to be Newtonian and hence its stress tensor takes the form:

$$\mathbb{T} = (-p + \lambda \operatorname{tr}\mathbb{D})\,\mathbb{1} + 2\mu\,\mathbb{D}, \tag{II.3}$$

where $\mathbb{D}$ is the rate of strain tensor, i.e. $\mathbb{D} = (\nabla \boldsymbol{u} + \nabla \boldsymbol{u}^T)/2$. Finally, μ and λ are the viscosity coefficients.

B. Boundary conditions (BCs)

A no-slip BC is imposed along the bottom, $\partial\Omega_B$. Along the free surface, both kinematic and dynamic BCs should be fulfilled. The kinematic free-surface BC is satisfied because of the lagrangian nature of the SPH.

The stress on the fluid domain boundaries $\partial\Omega$ is:

$$\mathbb{T}\boldsymbol{n} = [-p + \lambda \operatorname{div}(\boldsymbol{u})]\,\boldsymbol{n} + \mu\,(\boldsymbol{n}\times\boldsymbol{\omega}) + 2\mu\,\nabla\boldsymbol{u}\,\boldsymbol{n} \tag{II.4}$$

In this work, the surface tension is considered negligible, therefore, null stresses on free surface are enforced. This means that on $\partial\Omega_F$ the stress is zero and therefore the following equality holds:

$$[p - \lambda \operatorname{div}(\boldsymbol{u})]\boldsymbol{n}_F + \mu\,(\boldsymbol{\omega}\times\boldsymbol{n}_F) = 2\mu\,\frac{\partial \boldsymbol{u}}{\partial n} \tag{II.5}$$

where the pressure and the friction stress components balance the stress term due to the deformation of the free surface.

Eq. (II.5) can be split in the normal and tangential components by projecting it on the normal vector to the free surface $\boldsymbol{n}_F$ and on the free surface tangent hyperplane, which, in 2D, is defined by its tangent vector $\boldsymbol{\tau}_F$ (Fig. 1). Equation (II.5) can be then rearranged as:

$$\begin{cases} p = \lambda \operatorname{div}(\boldsymbol{u}) + 2\mu\,\dfrac{\partial \boldsymbol{u}}{\partial n}\cdot\boldsymbol{n}_F \\ \\ \boldsymbol{\omega}\cdot(\boldsymbol{\tau}_F\times\boldsymbol{n}_F) = -2\,\dfrac{\partial \boldsymbol{u}}{\partial n}\cdot\boldsymbol{\tau}_F \end{cases} \qquad \forall \boldsymbol{r}\in\partial\Omega_F \tag{II.6}$$

which are the two dynamic free-surface boundary conditions. The pressure and the vorticity on the free surface are linked by its geometrical configuration and the fluid normal velocity gradients [7].

Considering that the stress on the free surface is zero together with the eq. (II.3) we get that $\boldsymbol{\tau}\cdot\mathbb{D}\boldsymbol{n} = 0$, which implies:

$$\frac{\partial \boldsymbol{u}}{\partial \tau}\cdot\boldsymbol{n}_F + \frac{\partial \boldsymbol{u}}{\partial n}\cdot\boldsymbol{\tau}_F = 0. \tag{II.7}$$

This allows to change the normal derivatives in the second eq. of (II.6) in tangential derivatives.

In particular, in 2D, the latter becomes:

$$\omega \overset{2D}{=} 2\,\frac{\partial \boldsymbol{u}}{\partial \tau}\cdot\boldsymbol{n}_F = 2\,\frac{\partial u_n}{\partial \tau} - 2\,u_\tau\,\kappa, \tag{II.8}$$

being κ the curvature of the free surface in the considered point and $[u_\tau, u_n]$ the corresponding tangential and normal components of the velocity field.

III. Energy Conservation

A. General

The power that the fluid delivers or receives from the solid boundary $\partial\Omega_B$ is given by integrating the elementary power acting on each surface element of $\partial\Omega_B$, due to the stress forces. Denoting by $\boldsymbol{n}$ the unit normal vector pointing out of the fluid domain we get:

$$\mathcal{P}_{fluid/body} = -\int_{\partial\Omega_B} \mathbb{T}\boldsymbol{n}\cdot\boldsymbol{u_B}\,dS \tag{III.9}$$

The power $-\mathcal{P}_{fluid/body} = \mathcal{P}_{body/fluid} := \mathcal{P}_{ext}$ has to be converted into the total energy of the fluid. The surface integral (III.9) can be extended to the whole boundary $\partial\Omega$ since no power can act on the fluid through the free surface. An equivalent way to define the power using the divergence theorem gives therefore:

$$\mathcal{P}_{ext} = \int_\Omega \operatorname{div}(\mathbb{T}\boldsymbol{u})dV \tag{III.10}$$

The rhs of eq. (III.10) can be expressed as :

$$\mathcal{P}_{ext} = \int_\Omega (\operatorname{div}\mathbb{T})\cdot\boldsymbol{u}dV + \int_\Omega \mathbb{T}:\mathbb{D}\,dV \tag{III.11}$$

The external power is therefore separated in two different parts. In the present work the external power $\mathcal{P}_{ext}$ is assumed zero.

Using momentum conservation (second equation of II.1) and assuming that the body force $\boldsymbol{f}$ admits a potential field F so that $\nabla F = \boldsymbol{f}$, the first term of the lhs of (III.11) can be expressed as:

$$\int_\Omega \operatorname{div}(\mathbb{T})\cdot\boldsymbol{u}\,dV = \dot{\mathcal{E}}_P + \dot{\mathcal{E}}_K \tag{III.12}$$

being $\mathcal{E}_P$ and $\mathcal{E}_K$ respectively the potential and the kinetic energy. Their sum gives the mechanical energy:

$$\mathcal{E}_M := \mathcal{E}_P + \mathcal{E}_K \tag{III.13}$$

The second term of the rhs of (III.11) is the internal energy time derivative $\dot{\mathcal{E}}_I$. It can be expressed as:

$$\dot{\mathcal{E}}_I = \int_\Omega \mathbb{T}:\mathbb{D}\,dV = \mathcal{P}_C - \mathcal{P}_D - \mathcal{P}_B^\lambda, \tag{III.14}$$

where the four terms in the rhs are:

$$\begin{cases} \mathcal{P}_D := -2\mu\displaystyle\int_\Omega \mathbb{D}:\mathbb{D}\,dV \\ \\ \mathcal{P}_C := -\displaystyle\int_\Omega p\operatorname{div}(\boldsymbol{u})\,dV \\ \\ \mathcal{P}_B^\lambda := -\lambda\displaystyle\int_\Omega [\operatorname{div}(\boldsymbol{u})]^2\,dV \end{cases} \tag{III.15}$$

The power $\mathcal{P}_C$ is associated with the fluid compressibility and is a pure reversible term. Using the equation of state and the continuity equation, by integration, $\mathcal{P}_C$ can be reshaped as a potential energy (*i.e.* $\mathcal{P}_C = \dot{\mathcal{E}}_C$). In the case where a simple linear state equation is used, this term becomes:

$$\mathcal{E}_C(\rho) = \mathcal{E}_C(\rho_0) + c_0^2\int_\Omega \left[\log\left(\frac{\rho}{\rho_0}\right) + \frac{\rho_0}{\rho} - 1\right]\rho\,dV \tag{III.16}$$

where $\mathcal{E}_C(\rho_0)$ is the internal energy value set for the fluid at rest condition (*i.e.* $\rho = \rho_0$).

$\mathcal{P}_B^\lambda$ is the dissipative power caused by the fluid compressibility and it is negligible within the weakly compressible regime [5]. $\mathcal{P}_D$ is the classical viscous dissipation term for a Newtonian fluid.

Therefore, assuming $\mathcal{P}_{ext} = 0$ and $\mathcal{P}_B^\lambda \approx 0$ eq. (III.11) can be written as:

$$\dot{\mathcal{E}}_M + \dot{\mathcal{E}}_C = \mathcal{P}_D \leq 0 \tag{III.17}$$

the sum of the power due to the inertial force and the power associated to the reversible compressibility is balanced by the power dissipated by the fluid.

B. decomposition of the viscous dissipation term

Using the definition of $\mathcal{P}_D$ (equation III.15) and adding and subtracting the enstrophy, such term can be written as:

$$\mathcal{P}_D = -2\mu \int_\Omega (\nabla \boldsymbol{u} : \nabla^T \boldsymbol{u})\, dV - 2\mu \int_\Omega \boldsymbol{\omega}^2/2\, dV \tag{III.18}$$

To proceed in the analysis it is useful to consider the relation:

$$\nabla \boldsymbol{u} : \nabla^T \boldsymbol{u} = \nabla \cdot (\nabla \boldsymbol{u} \boldsymbol{u}) - \nabla(\mathrm{div}(\boldsymbol{u})) \cdot \boldsymbol{u}\,. \tag{III.19}$$

Using the equation (III.19) and the divergence theorem, eq. (III.18) becomes:

$$\mathcal{P}_D = -2\mu \int_{\partial\Omega} (\nabla \boldsymbol{u}\, \boldsymbol{u}) \cdot \boldsymbol{n}\, dS - \mu \int_\Omega \boldsymbol{\omega}^2\, dV + 2\mu \int_\Omega \nabla(\mathrm{div}(\boldsymbol{u})) \cdot \boldsymbol{u}\, dV \tag{III.20}$$

The divergence theorem can be applied on the last term and eq. (III.20) can be reshaped as:

$$\mathcal{P}_D = \mathcal{P}_{FS} + \mathcal{P}_{wall} + \mathcal{P}_B^\mu + \mathcal{P}_\omega \tag{III.21}$$

where the four terms in the rhs are:

$$\begin{aligned}
\mathcal{P}_{FS} &:= 2\mu \int_{\partial\Omega_F} [-(\nabla \boldsymbol{u}\, \boldsymbol{u}) \cdot \boldsymbol{n} + \mathrm{div}(\boldsymbol{u})(\boldsymbol{u} \cdot \boldsymbol{n})]\, dS \\
\mathcal{P}_{wall} &:= 2\mu \int_{\partial\Omega_B} [-(\nabla \boldsymbol{u}\, \boldsymbol{u}_B) \cdot \boldsymbol{n} + \mathrm{div}(\boldsymbol{u})(\boldsymbol{u}_B \cdot \boldsymbol{n})]\, dS \\
\mathcal{P}_B^\mu &:= -\mu \int_\Omega [\mathrm{div}(\boldsymbol{u})]^2\, dV\,. \\
\mathcal{P}_\omega &:= -\mu \int_\Omega \boldsymbol{\omega}^2\, dV
\end{aligned} \tag{III.22}$$

For the sake of simplicity, in this work, the body surfaces are assumed to be fixed (*i.e* $\boldsymbol{u}_B = 0$) and therefore $\mathcal{P}_{wall}$ is zero. The term $\mathcal{P}_B^\mu$ similarly to $\mathcal{P}_B^\lambda$ can be neglected in the weakly compressible regime. The volume integral term $\mathcal{P}_\omega$ is the dissipation due to the enstrophy while $\mathcal{P}_{FS}$ is a power linked to the deformation of the fluid domain due to the free surface motion.

Rearranging eq. (III.22) and eq. (III.17) in the present framework we get the energy balance:

$$\dot{\mathcal{E}}_M + \dot{\mathcal{E}}_C = \mathcal{P}_{FS} + \mathcal{P}_\omega \tag{III.23}$$

In the next section a brief description of how the above terms can be evaluated at the discrete level, with SPH, is given. Equation (III.23) is then used for studying the time evolution of a viscous standing wave. We show how the free-surface term $\mathcal{P}_{FS}$ and the enstrophy term $\mathcal{P}_\omega$ depend on the Reynolds number and on the wave amplitude.

IV. Conservation of energy in the SPH framework

A. SPH scheme

The SPH scheme adopted in this work is:

$$\begin{cases}
\dfrac{D\rho_i}{Dt} = -\rho_i \displaystyle\sum_j \frac{m_j}{\rho_j} (\boldsymbol{u}_j - \boldsymbol{u}_i) \cdot \nabla_i W_{ij} \\
\dfrac{D\boldsymbol{u}_i}{Dt} = - \displaystyle\sum_j \frac{m_j}{\rho_i \rho_j} (p_j + p_i) \nabla_i W_{ij} + \mu \sum_j \frac{m_j}{\rho_i \rho_j} \pi_{ij} \nabla_i W_{ij} + \boldsymbol{g}_i \\
\dfrac{De_i}{Dt} = -p_i \displaystyle\sum_j \frac{m_j}{\rho_i \rho_j} (\boldsymbol{u}_j - \boldsymbol{u}_i) \cdot \nabla_i W_{ij} + \mu \sum_j \frac{m_j}{\rho_i \rho_j} \pi_{ij} (\boldsymbol{u}_j - \boldsymbol{u}_i) \cdot \nabla_i W_{ij} \\
\dfrac{D\boldsymbol{r}_i}{Dt} = \boldsymbol{u}_i(t), \qquad p = c_0^2(\rho - \rho_0)
\end{cases} \tag{IV.24}$$

with

$$\pi_{ij} = K \frac{(\boldsymbol{u}_j - \boldsymbol{u}_i) \cdot (\boldsymbol{r}_j - \boldsymbol{r}_i)}{\|\boldsymbol{r}_j - \boldsymbol{r}_i\|^2} \tag{IV.25}$$

where $K = 2(n+2)$ and n is the spatial dimension of the problem at hand, ρ_i, p_i, e_i, $\boldsymbol{u}_i$ and m_i are respectively the density, the pressure, the internal energy, the velocity and the mass of the i-th particle. The body force term $\boldsymbol{f}$ takes here the form of standard gravity acceleration $\boldsymbol{g} = -g\boldsymbol{k}$, $\boldsymbol{k}$ being the unit vector in the z direction. It has to be remarked that energy conservation has been included in order to track the evolution of the internal energy.

B. SPH approximation of energy integrals

Linear momentum and energy are exactly conserved in the present SPH scheme. Considering the particle system on the SPH model, the mechanical and internal energies of the fluid domain are computed in SPH as:

$$\mathcal{E}_M^{\text{SPH}} = \sum_i \left(m_i \frac{\boldsymbol{u}_i^2}{2} + m_i\, g\, z_i \right), \qquad \mathcal{E}_I^{\text{SPH}} = \sum_i m_i\, e_i \tag{IV.26}$$

where the specific internal energy of he i-th particle is given by the energy equation in system (IV.24). The total internal energy variation is hence:

$$\begin{aligned}
\dot{\mathcal{E}}_I^{\text{SPH}} = &- \sum_i \sum_j \frac{m_i m_j}{\rho_i \rho_j} p_i (\boldsymbol{u}_j - \boldsymbol{u}_i) \cdot \nabla_i W_{ij} + \\
&+ \mu \sum_i \sum_j \frac{m_i m_j}{\rho_i \rho_j} \pi_{ij} (\boldsymbol{u}_j - \boldsymbol{u}_i) \cdot \nabla_i W_{ij}
\end{aligned} \tag{IV.27}$$

The first term in the right-hand side is linked to the power component $\mathcal{P}_C$, due to the compressibility, and the second is connected to viscous components $\mathcal{P}_D$ and $\mathcal{P}_B^\mu$. Following the definition given in section III at continuum, it is possible to define the two power components:

$$\begin{cases}
\mathcal{P}_C^{\text{SPH}} = - \displaystyle\sum_i \sum_j \frac{m_i m_j}{\rho_i \rho_j} p_i (\boldsymbol{u}_j - \boldsymbol{u}_i) \cdot \nabla_i W_{ij} \\
\mathcal{P}_{D+B}^{\text{SPH}} = -\mu \displaystyle\sum_i \sum_j \frac{m_i m_j}{\rho_i \rho_j} \pi_{ij} (\boldsymbol{u}_j - \boldsymbol{u}_i) \cdot \nabla_i W_{ij}
\end{cases} \tag{IV.28}$$

As shown in [8], it is not possible to separate the two components $\mathcal{P}_D$ and $\mathcal{P}_B^\mu$ in the SPH viscous operator and for this reason the notation $\mathcal{P}_{D+B}^{\text{SPH}}$ is kept in the following. Furthermore, in [8] it is demonstrated that the SPH viscous operator adopted in the present scheme forces the constraint $\lambda = \mu$. Therefore the limit for the convergence of $\mathcal{P}_{D+B}^{\text{SPH}}$ is

$$\lim_{h\to 0;N\to\infty} \mathcal{P}_{D+B}^{\text{SPH}} = \mathcal{P}_D + \mathcal{P}_B^\mu \tag{IV.29}$$

Substituting the equation of state (II.2) and the SPH continuity equation in $\mathcal{P}_C^{\text{SPH}}$, after some math, it is possible to recover the equation III.16 at the discrete level:

$$\mathcal{E}_C^{\text{SPH}} = \mathcal{E}_C^{\text{SPH}}(\rho_0) + c_0^2 \sum_i m_i \left[\log\left(\frac{\rho_i}{\rho_0}\right) + \frac{\rho_0}{\rho_i} - 1 \right]. \tag{IV.30}$$

Equation (IV.27) can be rewritten in a compact way as:

$$\dot{\mathcal{E}}_I^{\text{SPH}} = \dot{\mathcal{E}}_C^{\text{SPH}} - \mathcal{P}_{D+B}^{\text{SPH}}. \tag{IV.31}$$

Thanks to the symmetry property of the kernel function it is possible to demonstrate that the system (IV.24) conserves exactly the energy of the particle system (see *e.g.* [9]):

$$\dot{\mathcal{E}}_M^{\text{SPH}} + \dot{\mathcal{E}}_I^{\text{SPH}} = 0 \tag{IV.32}$$

Considering that the viscous operator used in the present SPH model is a pure dissipative term (see *e.g* [10],) it follows that:

$$\dot{\mathcal{E}}_M^{\text{SPH}} + \dot{\mathcal{E}}_C^{\text{SPH}} = \mathcal{P}_{D+B}^{\text{SPH}} \leq 0 \tag{IV.33}$$

therefore, the second law of thermodynamics is respected at the discrete level.

With the exception of kinetic energy, potential energy and compressible energy, the terms are defined as a power in these sections. The power terms are directly derived from the numerical equations or from interpolations on the data (see next subsection). In order to quantify the dissipation of energy connected to the different effects along a simulation, it is useful to integrate the power terms in time. In the following $\Delta\mathcal{E}_X^Y$ is a notation referred to the definition:

$$\Delta\mathcal{E}_X^Y(t) = \int_{t_0}^{t} \mathcal{P}_X^Y \, dt \tag{IV.34}$$

In the next sections, the energy dissipated by the particle system, at the end of the simulation, is made non dimensional using the mechanical energy given at the initial condition. The ratio $\Delta\mathcal{E}_{D+B}^{\text{SPH}}(t_f)/\mathcal{E}_{M0}$ gives in this way a clear indication of the dissipation level attained at the end time, t_f, of the period of interest.

C. Energy components through Moving Least Square interpolation on scattered data

From the previous section it has been shown that from the SPH equation it is possible to identify the main energy components. Those components can be also derived using Moving Least Square (MLS) interpolation formula for scattered data. In particular in this work a first order MLS formula is used in the following (see *e.g.* [11], [12]). Through this formula, the velocity gradient, $\langle\nabla\boldsymbol{u}\rangle^{\text{MLS}}$, divergence and vorticity fields, $\langle\text{div}(\boldsymbol{u})\rangle^{\text{MLS}}$, $\langle\omega\rangle^{\text{MLS}}$, can be retrieved form the SPH outputs (*i.e.* from the particle positions, velocities and volumes):

$$\begin{cases} \langle\nabla\boldsymbol{u}\rangle^{\text{MLS}}(\boldsymbol{r}_i) = \sum\limits_{j\in Fluid} \boldsymbol{u}_j \otimes \nabla W_{ij}^{\text{MLS}} V_j \\ \langle\omega\rangle^{\text{MLS}}(\boldsymbol{r}_i) = \sum\limits_{j\in Fluid} \boldsymbol{u}_j \times \nabla W_{ij}^{\text{MLS}} V_j \\ \langle\text{div}\boldsymbol{u}\rangle^{\text{MLS}}(\boldsymbol{r}_i) = \sum\limits_{j\in Fluid} \boldsymbol{u}_j \cdot \nabla W_{ij}^{\text{MLS}} V_j \end{cases} \tag{IV.35}$$

Eqs. (IV.35) are necessary to directly evaluate, from eqs. (III.22), the power components related to enstrophy, $\mathcal{P}_\omega^{\text{MLS}}$, and to free surface, $\mathcal{P}_{FS}^{\text{MLS}}$.

D. Free surface terms

In section (III-B), it is shown how the viscous dissipation can be decomposed in a volume integral $\mathcal{P}_\omega^{\text{MLS}}$ and a boundary integral $\mathcal{P}_{FS}$ on the free surface. The discrete and lagrangian nature of SPH makes unclear the definition of a discrete free-surface integral and its evaluation is not straightforward for the following reasons: i)

1) particles belonging to the free-surface need to be detected and, as shown in [13], this identification is not unique but depends on the specific algorithm and from the parameters connected with it.
2) once the particles on the free surface have been identified, it is necessary to calculate the normal vector to this surface
3) if the free surface is highly fragmented it can be difficult to perform connections needed for the surface integration (see *e.g.* [14])

Using the algorithm proposed in [13], a subset of particles FS belonging to the free surface can be defined. The algorithm gives also the evaluation of the normal vector field, and the surface integral $\mathcal{P}_{FS}$ defined by eq. III.22 can be approximated as:

$$\mathcal{P}_{FS}^{\text{MLS}} := 2\mu \sum_{k\in FS} \left[\langle\text{div}(\boldsymbol{u})\rangle_k^{\text{MLS}} \boldsymbol{u}_k - \langle\nabla\boldsymbol{u}\rangle_k^{\text{MLS}} \boldsymbol{u}_k \right] \cdot \boldsymbol{n}_k \, \Delta S_k \tag{IV.36}$$

where the length of the surface elements is simply approximated as $\Delta S_k = (V_k)^{1/n_{Dim}}$. Also for Eq. (IV.36) the MLS interpolation is needed to evaluate the velocity gradient for the particles involved in. When the free surface is highly fragmented, the free-surface terms defined in (IV.36) can be inaccurate. Under such conditions the surface integral $\mathcal{P}_{FS}$ can be evaluated by subtraction using the energy balance (III.23), the relation (IV.33), and the MLS interpolation (IV.35) for evaluating the enstrophy term $\mathcal{P}_\omega^{\text{MLS}}$:

$$\mathcal{P}_{FS}^{sub} := \mathcal{P}_{D+B}^{\text{SPH}} - \mathcal{P}_\omega^{\text{MLS}} \tag{IV.37}$$

where the superscript *sub* is used to differentiate this term from the one calculated through (IV.36).

It has to be remarked that due to the exact energy conservation of the SPH scheme, the errors in eq. (IV.37) arise exclusively from those of the MLS interpolation for the integrand of the enstrophy term $\mathcal{P}\omega$ in eqs. (III.22). On the other hand,

the evaluation of $\mathcal{P}_{FS}^{\text{MLS}}$ through the summation (IV.36) is more complex since it involves the MLS interpolation, detection of free-surface particles and evaluation of free-surface normal and surface elements.

V. Numerical tests

A. General

The problem investigated in this section is the viscous attenuation of a standing wave in deep water condition. Periodic conditions are used for the vertical boundaries while the sea bottom is modelled through a solid flat surface where no-slip condition is enforced (see Fig. 1). Because of the deep water condition, the bottom solid boundary has a negligible role and therefore the vorticity field is mainly concentrated near the free surface. In order to discuss the influence of viscosity on the components $\mathcal{P}_{FS}$ and $\mathcal{P}_{\omega}$, a range of Reynolds numbers, Re $\in [125-2000]$, has been considered. In addition, the non-linear effects connected to large wave amplitudes, A, are investigated. Indeed, for large amplitude the free surface starts to break inducing large effects on the components $\mathcal{P}_{FS}$ and $\mathcal{P}_{\omega}$. For this first test-case, and for all the combination (A,Re) investigated, the term $\mathcal{P}_{FS}$ remains always dominant with respect to $\mathcal{P}_{\omega}$.

The damping of viscous gravity waves has been recently studied in [15] where an analytical solution of the linearized Navier-Stokes equation has been derived for a wide range of Reynolds numbers and water depths. In [5] the same problem has been considered in the framework of the SPH model where it is shown that, using a proper spatial resolutions and a proper number of interacting neighbours, a good agreement between SPH and the analytical solution can be obtained. In the present work this previous analysis is extended to analyse varying the Reynolds number and to the wave amplitude. In particular the maximum wave steepness considered in this work is larger than the breaking limit $kA = 0.68$ (see *e.g.* [16]), being A the wave amplitude and k the wave number. In this way, the effect of breaking wave on the viscous dissipation can be also discussed for this scenario.

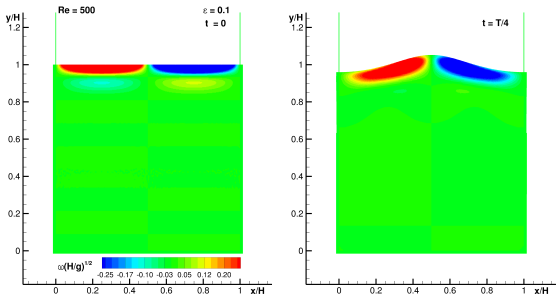

Fig. 2. Vorticity field for the standing wave problem for two time instants $t = 0$ and $t = T/4$, being T the linear theory period of oscillation [16].

Figure 2 describes the initial configuration of the problem. Here, L is the wave length and $H = L$ is the still water depth, the dimensionless wave number kH is therefore equal to 2π. Note that the latter value means that the analysis is performed in a deep water regime (*i.e.* $kH \geq \pi$). The boundary layer of the free-surface is well visible from the vorticity fields plotted in Fig. 2 while the bottom boundary layer is not visible in the range of values used because of the deep water regime. As a consequence, the effect of the bottom boundary layer can be neglected, hence simplifying the analysis.

The free surface is initially flat in order to simplify particle positioning. The initial pressure and velocity fields were evaluated using the analytical solution of [15]. The initial value of the mechanical energy is computed and denoted as $\mathcal{E}_{M0}$. The potential energy is set equal to zero at the initial time (*i.e.* $\mathcal{E}_{M0} = \mathcal{E}_{K0}$). The amplitude of the standing wave is set through the parameter $\epsilon = 2A/L$. The Reynolds number for this problem is defined as $\text{Re} = H\sqrt{gH}/\nu$ to avoid dependencies of ϵ on this parameter. Five Reynolds numbers and four wave amplitudes are investigated to describe different dissipation laminar regimes. The period of oscillation, T, depends on the two parameters Re and ϵ. For high Re and small ϵ, T is close to the predicted by linear theory [16], $T_{lin} = 2\pi/\sqrt{gk}$. Since $kH = 2\pi$ in present example, $T_{lin} = \sqrt{2\pi}\sqrt{H/g}$. Taking advantage of this, $\sqrt{H/g}$ will be used to make time non-dimensional in some graphs.

For the SPH simulations presented in this subsection the maximum spatial resolution adopted is $H/\Delta x = 800$ (corresponding to a total number of particles equal to 640000) and the smoothing length is $h/\Delta x = 2.8$ (Wendland C2 kernel is used for all the simulations). Indeed, using these parameters the results presented in [5] are close to a convergence limit.

The final time of the simulations, hereinafter t_f, has been chosen (see Table I) large enough so that mechanical energy is dissipated until its value is approximately 1% of its initial value, $\mathcal{E}_{M0}$.

	t_f/T_{lin}	$\epsilon = 0.1$	0.2	0.3	0.4
Re = 125	2.4	1E-04	1.2E-03	3.2E-03	6.4E-03
Re = 250	4.0	1.9E-03	3.0E-03	5.2E-03	8.1E-03
Re = 500	6.4	7.2E-03	7.8E-03	1.1E-02	1.7E-02
Re = 1000	12	5.6E-03	6.3E-03	7.6E-03	1.1E-02
Re = 2000	20	6.4E-03	1.1E-02	1.1E-02	7.1E-03

TABLE I
Energy dissipated at the end of the simulation with respect to the initial value $\mathcal{E}_{M0}$: *i.e.* $[\mathcal{E}_{M0} - \Delta\mathcal{E}_{D+B}^{\text{SPH}}(t_f)]/\mathcal{E}_{M0}$.

When a low viscosity liquid like water is considered, the velocity field associated with a gravity wave can be considered practically irrotational and divergence free. Therefore, such velocity field can be expressed through a potential velocity, *i.e.*, $\boldsymbol{u} = \nabla\Phi$. Under these conditions, $\mathcal{P}_{\omega}$ is negligible and the viscous dissipation can be expressed using only the component $\mathcal{P}_{FS}$ which becomes:

$$\mathcal{P}_D \simeq \mathcal{P}_{FS} \simeq -2\mu \int_{\partial\Omega_F} \nabla\nabla\Phi\,\nabla\Phi \cdot \boldsymbol{n}\, dS \simeq -2\mu \int_0^L \left(\Phi_{xy}\,\Phi_x + \Phi_{yy}\,\Phi_y\right) dx \tag{V.38}$$

where the right hand side, is a linearized approximation valid for small ϵ. This is the relation used in [17] (see pag. 234) to estimate the viscous damping of water waves.

This consideration highlights that, for gravity wave dynamics, $\mathcal{P}_{FS}$ is generally dominant with respect to $\mathcal{P}_{\omega}$. In the next subsections we show how those two contributions change with the viscosity of the flow and the intensity of the velocity field given in the initial condition.

B. High viscosity & small amplitude: Re=125, ϵ = 0.1

For this case, the initial energy $\mathcal{E}_{M0}$ is mostly dissipated (about 80%) by the viscous effects in just one oscillation cycle.

Figure 3 displays the evolution in time of the kinetic energy $\mathcal{E}_K$ and the dissipation caused by enstrophy $\Delta\mathcal{E}_{\omega}$. From the analytic solution of [15], in addtion to $\mathcal{E}_K(t)$, the enstrophy term $\Delta\mathcal{E}_{\omega}(t)$ value is also given. The SPH predictions are in good agreement with the analytical ones. For this case, at the end of the simulation, the dissipation associated with enstrophy amounts to 40% of the total dissipation. It is remarkable that, with a so high viscosity fluid, the free surface term is still the dominant one.

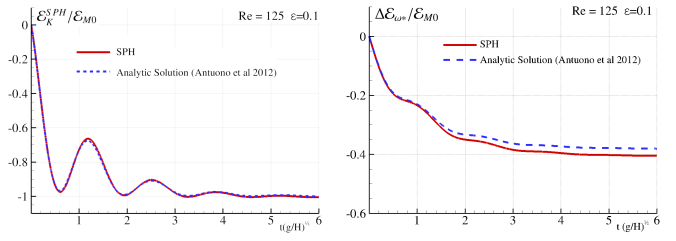

Fig. 3. Left: Kinetic energy, $\mathcal{E}_K(t)$ as a function of time for Re=125 ϵ=0.1. Right: Dissipation linked to enstrophy $\Delta\mathcal{E}_{\omega}(t)$ as a function of time.

C. High viscosity & large amplitude: Re=125, ϵ = 0.4

Snapshots of the vorticity field are pictured in Figure 4. Because of the high viscosity, the breaking of the free surface is however inhibited.

The vorticity is generated at the free-surface. Indeed, the boundary condition (II.8) requires $\omega = 2\,\partial u_n/\partial\tau$, which remains confined on the free-surface boundary layer and is partially diffused inside the field during the wave oscillations. During each period the vorticity intensity decreases due to the mechanical energy dissipation.

Compared to the previous low amplitude case, the kinetic energy ratio $\Delta\mathcal{E}_k/\mathcal{E}_{M0}$ presents a slightly less sudden decrease while the period of oscillation increases (left plot of Figure 5). Nevertheless, also in this case the initial energy is, to a high extent, dissipated in the first wave oscillation. The component due to the enstrophy $\Delta\mathcal{E}_{\omega}/\mathcal{E}_{M0}$ behaves similarly, being slightly larger level just during the first cycle (right plot of figure 5). These results show that the change in the amplitude, ϵ, has a limited effect on the behaviour of the energy decay. The final value of $\Delta\mathcal{E}_{\omega}$ is close to 40% of the initial energy $\mathcal{E}_{M0}$ for both amplitude ratios, ϵ, analysed. In next section, it is shown that this is not the case when increasing the Reynolds number because of the breaking wave events.

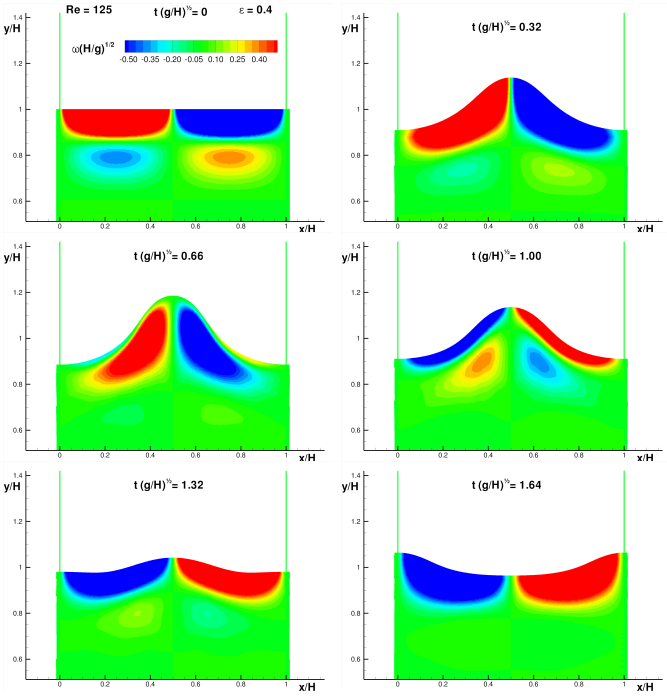

Fig. 4. Vorticity field, Re=125, ϵ=0.4.

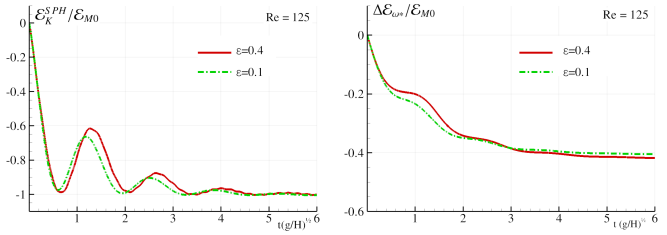

Fig. 5. Kinetic energy $\Delta\mathcal{E}_k$ (left) and dissipation term $\Delta\mathcal{E}_{\omega}$ as as a function of time, Re=125, ϵ=0.1, 0.4.

The energy term $\Delta\mathcal{E}_{FS}$, evaluated through $\Delta\mathcal{E}_{FS}^{\text{MLS}}$, eq. (IV.36), and through $\Delta\mathcal{E}_{FS}^{sub}$, is plotted in time in Figure 6. The difference between the two plots is around 0.2% in relative terms, which means that the parameters used for the numerical simulations allow to solve in a good way the present test-case.

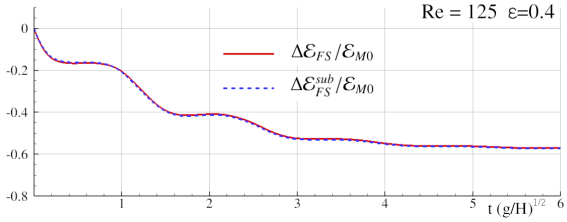

Fig. 6. Dissipation through the free surface term, $\Delta\mathcal{E}_{FS}$ as a function of time, Re=125, ϵ=0.4. Direct computation, eq. (IV.37), and subtraction, eq. (III.23).

D. Low viscosity & small amplitude: Re=2000, $\epsilon = 0.1$

In this third test case the viscosity of the fluid is highly reduced setting the Reynolds number equal to 2000. In this condition the free-surface boundary layer becomes much thinner compared to the previous cases and therefore the spatial resolution needs to be set adequately to resolve this region. The mechanisms are globally the same than those observed in the, equal amplitude, more viscous case of section V-B, but in this case more than ten periods of oscillation are needed to dissipate 80% of the initial energy $\mathcal{E}_{M0}$.

Left panel of Figure 7 presents the comparison with the analytical solution of [15] in terms of kinetic energy decay. The matching between the two curves is very good similarly to what is shown in [5] in the same range of Reynolds numbers. Right plot of figure 7 depicts he comparison with the analytical solution of [15] in terms of the enstrophy component $\mathcal{E}_\omega$. For this test-case the latter reduces to only 7% and therefore the dissipation in mainly due to the free-surface component $\mathcal{E}_{FS}$.

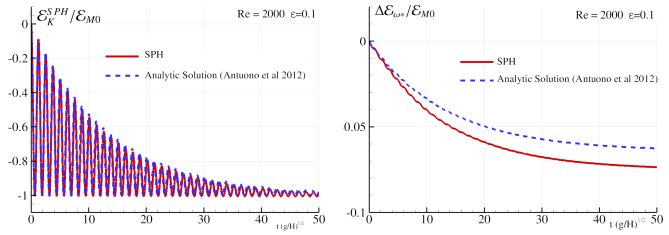

Fig. 7. Kinetic energy $\Delta\mathcal{E}_k$ (left) and dissipation term $\Delta\mathcal{E}_\omega$ as as a function of time, Re=2000, ϵ=0.1.

E. Low viscosity & large amplitude: Re=2000, $\epsilon = 0.4$

For this case large deformations of the free surface occur. They induce in the first cycle the formation of an overturning wave and a subsequent plunging breaking event. Some snapshots during the time evolution are reported in Figure (8).

To resolve accurately the breaking event, the spatial resolution has been doubled, ($H/\Delta x = 800$).

Left plot of Figure 9 shows the kinetic energy decay for the two wave amplitudes, $\epsilon = 0.1$ and $\epsilon = 0.4$. For the latter the dissipation process is much faster; being this fact related to the breaking phenomena, which induces extra dissipation. As a matter of fact, due to the vorticity entrapped by the breaking, the enstrophy component $|\Delta\mathcal{E}_\omega|$ largely increases when compared to the small amplitude case (right plot of Figure 9). The collapse of the entrapped cavities (last snapshots of Figure 8) induces a sudden decrease of $\Delta\mathcal{E}_\omega$, with around 8% of the whole kinetic energy being lost in one breaking event. These significant energy losses had been predicted by Szymczak [18] in the context of liquid jets impacting on solid walls.

Finally, Figure 10 depicts the time evolution of term $\Delta\mathcal{E}_{FS}$ evaluated through $\Delta\mathcal{E}_{FS}^{\text{MLS}}$, eq. (IV.36), and through $\Delta\mathcal{E}_{FS}^{sub}$. It is remarkable that the two plots are in a fair agreement even for this complex case, with breaking phenomena, which make the evaluation of the surface integral (IV.36) more difficult.

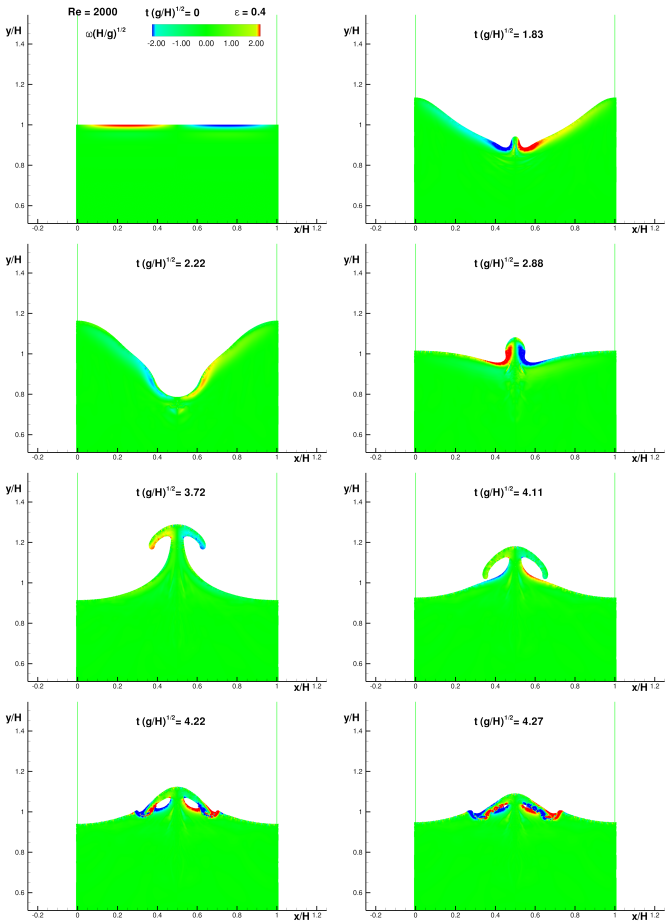

Fig. 8. Vorticity field, Re=2000, ϵ=0.4, $H/\Delta x = 800$.

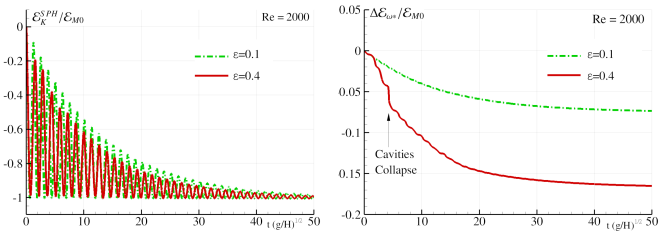

Fig. 9. Kinetic energy as a function of time, Re=2000, ϵ=0.4.

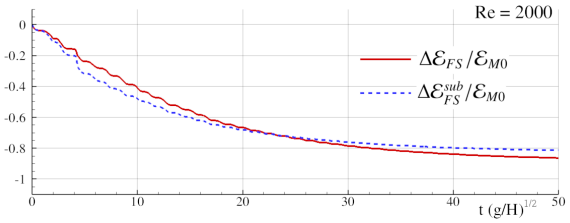

Fig. 10. Dissipation through the free surface term as a function of time, Re=2000, ϵ=0.4.

F. Summary of the influence of the Reynolds number and the wave amplitude on the viscous dissipation

In previous sections, four cases of matrix I have been discussed in detail, showing how the viscous dissipation distributes between the components $\Delta\mathcal{E}_\omega$ and $\Delta\mathcal{E}_{FS}$. The results of all 20 cases of that matrix are summarized in Figure 11, in which $\Delta\mathcal{E}_\omega$, measured at the end of the simulations, is plotted as a function of Reynolds number and wave amplitude. As the wave amplitude is set larger, the enstrophy component of dissipation, in modulus, tends to grow for all Reynolds numbers. However, this increase sees a drastic change for the highest Reynolds, for which large breaking takes place in the first period of oscillation. In this case, the vorticity generated by the cavities collapse induces a large increase of $|\Delta\mathcal{E}_\omega|$.

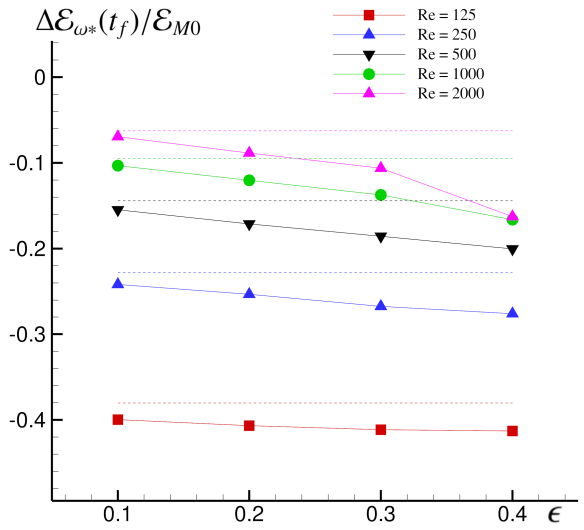

Fig. 11. Energy dissipation through enstrophy component $\Delta\mathcal{E}_\omega$ at the end of simulations, varying Re and ϵ. Dashed lines are analytical results from [15].

VI. Conclusions

An energy decomposition technique for viscous free-surface flows has been presented and applied to the WCSPH modelling of a standing wave, for which a matrix of cases, covering a large range of Reynolds numbers and wave amplitudes, has been set. For the high Reynolds and large amplitude case, wave breaking appears. Its influence in mechanical energy dissipation has been discussed. It has been found that:

1) The dissipated mechanical energy can be written as the sum of two terms: the enstrophy volume integral and a surface integral along the free surface.
2) Applying energy conservation, a double-checking of the free surface term is developed and applied, confirming the quality of the surface integral SPH evaluation, even in the presence of moderately fragmented free surface.
3) For low amplitude cases the free-surface contribution to dissipation is substantially larger than the enstrophy one.
4) For large amplitude cases, the flow becomes very energetic, eventually leading to steep and/or breaking waves.
5) In the case with wave breaking, the related vorticity generation, in the first breaking event, induces a mechanical energy dissipation of around 8% of the initial energy.

It remains as future work to apply the methodology presented in the paper to more complex fragmented free surface flows for which, the dissipated energy may influence the external dynamics of a building, vehicle, etc.. It remains also to compare the results with those of mesh based methods and to incorporate gas phase and surface tension in the analysis.

Acknowledgements

Work supported by Flagship Project RITMARE - Italian Research for the Sea - coordinated by Italian National Research Council and funded by Italian Ministry of Education, University and Research within Nat. Res. Program 2011-2014.

References

[1] L. M. Sun and Y. Fujino, "A semi-analytical model for tuned liquid damper (TLD) with wave breaking," *Journal of Fluids and Structures*, vol. 8, no. 5, pp. 471–488, 7 1994.
[2] A. Iafrati, "Numerical study of the effects of the breaking intensity on wave breaking flows," *Journal of Fluid Mechanics*, vol. 622, pp. 371–411, 3 2009.
[3] B. Bouscasse, A. Colagrossi, A. Souto-Iglesias, and J. L. Cercos-Pita, "Mechanical energy dissipation induced by sloshing and wave breaking in a fully coupled angular motion system. I. theoretical formulation and numerical investigation," *Physics of Fluids (1994-present)*, vol. 26, no. 3, 2014.
[4] ——, "Mechanical energy dissipation induced by sloshing and wave breaking in a fully coupled angular motion system. II. experimental investigation," *Physics of Fluids (1994-present)*, vol. 26, no. 3, 2014.
[5] A. Colagrossi, A. Souto-Iglesias, M. Antuono, and S. Marrone, "Smoothed-particle-hydrodynamics modeling of dissipation mechanisms in gravity waves," *Phys. Rev. E*, vol. 87, p. 023302, Feb 2013.
[6] P. Madsen and H. Schaffer, "A discussion of artificial compressibility," *Coastal Engineering*, vol. 53, no. 1, pp. 93 – 98, 2006.
[7] T. Lundgren and P. Koumoutsakos, "On the generation of vorticity at a free surface," *Journal of Fluid Mechanics*, vol. 382, pp. 351–366, 1999.
[8] A. Colagrossi, M. Antuono, A. Souto-Iglesias, and D. Le Touzé, "Theoretical analysis and numerical verification of the consistency of viscous smoothed-particle-hydrodynamics formulations in simulating free-surface flows," *Physical Review E*, vol. 84, pp. 26 705+, 2011.
[9] A. Colagrossi, G. Graziani, and M. Pulvirenti, "Particles for fluids: Sph vs vortex methods," *Journal of Mathematics and Mechanics of Complex Systems*, vol. 2, no. 1, pp. 45–70, 2014.
[10] D. Violeau, "Dissipative forces for lagrangian models in computational fluid dynamics and application to smoothed-particle hydrodynamics," *Phys. Rev. E*, vol. 80, p. 036705, Sep 2009.
[11] T. Fries and H. Matthies, "Classification and overview of meshfree methods," *Scientific Computing, Informatikbericht*, 2004.
[12] A. Colagrossi, "A meshless lagrangian method for free-surface and interface flows with fragmentation," Ph.D. dissertation, Università di Roma La Sapienza, 2005.
[13] S. Marrone, A. Colagrossi, D. L. Touzé, and G. Graziani, "Fast free-surface detection and level-set function definition in SPH solvers," *Journal of Comp. Physics*, vol. 229, no. 10, pp. 3652 – 3663, 2010.
[14] M. Antuono, A. Colagrossi, D. Le Touzé, and J. Monaghan, "Conservation of circulation in SPH for 2D free-surface flows," *Int. Journal for Num. Methods in Fluids*, vol. 72, no. 5, pp. 583–606, 2013.
[15] M. Antuono and A. Colagrossi, "The damping of viscous gravity waves," *Wave Motion*, vol. 50, no. 0, pp. 197–209, 2013.
[16] R. Dean and R. Dalrymple, *Water wave mechanics for engineers and scientists*, ser. Advanced series on ocean eng. World Scientific, 1991.
[17] J. Lighthill, *Waves in fluids*. Cambridge University Press, 2001.
[18] W. Szymczak, "Energy losses in non-classical free surface flows," in *Bubble Dynamics and Interface Phenomena*, ser. Fluid Mechanics and Its Applications, J. Blake, J. Boulton-Stone, and N. Thomas, Eds. Springer Netherlands, 1994, vol. 23, pp. 413–420.